American Mineralogist, Volume 66, pages 491–506, 1981

Progressive metamorphism of the chert-bearing Durness limestone in the Beinn an Dubhaich aureole, Isle of Skye, Scotland: A reexamination

ALICE L. HOERSCH

Department of Geology, La Salle College
Philadelphia, Pennsylvania 19141

Abstract

In the contact metamorphic aureole of the Beinn an Dubhaich granite, Isle of Skye, Scotland, nodular chert (70 percent quartz, 20 percent dolomite, 10 percent calcite) reacted with dolostone (99 percent dolomite, 1 percent calcite) to form reaction rims (mantles) of calc-silicate minerals. In general talc, tremolite, diopside, and forsterite appear successively in the reaction rims as the granite is approached. Mineral assemblages in the aureole can be related by equilibria in the system $CaO–MgO–SiO_2–CO_2–H_2O$ at $P_T = 500$ bars, P_T being the estimated lithostatic pressure at the time of granitic intrusion. Fluorine can be neglected as the molecular proportion of fluoro-talc and fluoro-tremolite is less than 0.017. The sequence of talc and tremolite reactions and their areal extent suggests that talc is stable at low pressures.

Two prograde reaction paths, indicating different $X(CO_2)$, can be traced at different zone boundaries within the nodules. One path corresponds to reactions within the mantle or at the matrix–mantle boundary. The other path corresponds to reactions at the core–mantle boundary and persisted as long as dolomite and quartz remained in the core of the nodules. Once quartz was consumed in the nodules the two paths converged. Small but significant fluid composition differences [$\sim 0.1\ X(CO_2)$] existed across the reaction rims, which are 1 mm to several cm wide. These $X(CO_2)$ differences reflect the buffering capacities of mineral assemblages at zone boundaries, and perhaps the opposing outward flow of CO_2-rich fluid derived from the reactions and inward flow of H_2O-rich matrix pore fluid. The two prograde paths equilibrated at $X(CO_2) > 0.85$ once talc was consumed.

Introduction

The contact metamorphic aureole of the Beinn an Dubhaich granite, Isle of Skye, Scotland, provides an excellent example of the growth of concentrically zoned calc-silicate rims around chert nodules in the Durness limestone. All stages of growth of the reaction rims are present in the aureole, from the onset of metamorphism, in which a thin reaction rind surrounds the chert nodules, to complete equilibration between the limestone and chert, so that no quartz remains in the nodules. These calc-silicate reaction rims, ranging in grade from talc to forsterite-bearing assemblages, were briefly examined by Tilley (1948b).

This paper describes the stages of growth of the reaction rims around the chert nodules, which in turn are used to trace prograde reaction paths on the pertinent $T–X(CO_2)$ diagram. These paths are extremely important in characterizing the composition and behavior of the fluid phase at all stages of rim growth and will also be used in a forthcoming paper describing diffusion that has taken place across the rims.

Another point that can be addressed by the study of the growth of these reaction rims concerns talc stability in siliceous dolomites at low pressures. Some controversy has existed as to whether the talc stability field decreases with decreasing pressure on $T–X(CO_2)$ diagrams, as inferred from experimental evidence by Skippen (1971, 1974), or whether it increases with decreasing pressure, as proposed by Slaughter *et al.* (1975) and Kerrick and Slaughter (1976). Several field studies provide data on phase relationships at pressures greater than 1–2 kbar (Trommsdorff, 1972; Puhan and Hoffer, 1973; Moore and Kerrick, 1976). This study concerns metamorphism at 275–575 bars total lithostatic pressure, and provides important data on the low-pressure phase relations.

0003–004X/81/0506–0491$02.00

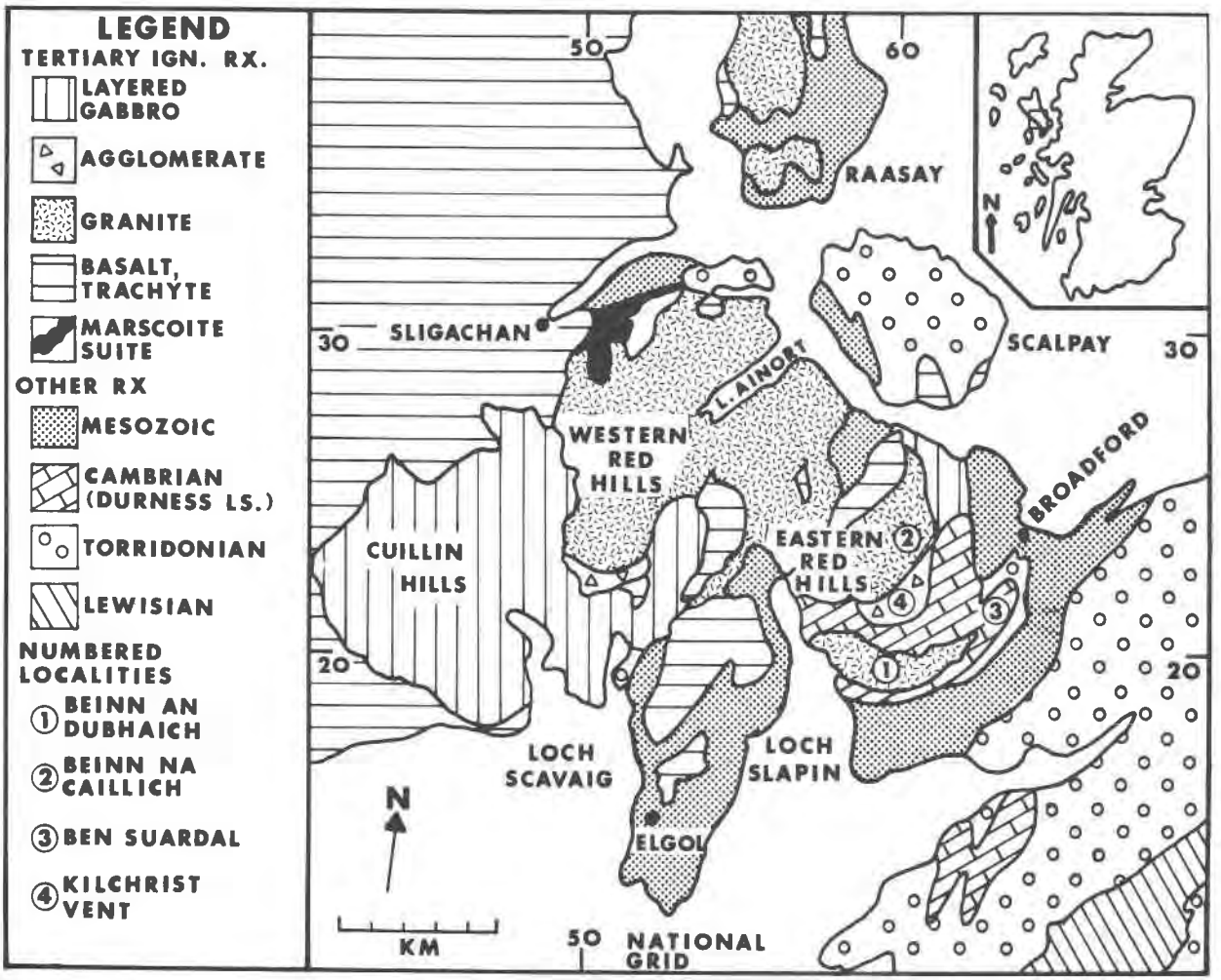

Fig. 1. Geologic map of southern Skye (after Moorbath and Bell, 1969).

Geologic setting

The Beinn an Dubhaich granite (Fig. 1), on the Isle of Skye off the northwest coast of Scotland, is part of a Tertiary igneous complex that includes intrusive gabbro (Cuillin Hills), granites (Eastern and Western Red Hills), and diabase dikes, as well as extrusive basalt flows. The granite, part of the Eastern Red Hills and approximately 4.5 km long and 1.2 km wide, intruded and metamorphosed Cambrian Durness limestone (Figs. 2, 3) and Torridonian sandstone. According to Rb–Sr age determinations of Moorbath and Bell (1965), the Beinn an Dubhaich granite is 55 ± 4 m.y., which makes it one of the youngest intrusives in the area. Another younger granite, the Beinn na Caillich granite, and the Kilchrist Vent, both of which are also part of the Eastern Red Hills, lie north of the Beinn an Dubhaich granite and also contributed to the metamorphism of the sediments lying between Beinn an Dubhaich and Beinn na Caillich. Several patches of granite within the sediments northeast of Beinn an Dubhaich also locally affected metamorphic grade.

Three main horizons of the Durness limestone are exposed in the contact aureole of the granite (Tilley, 1948b). They include (Fig. 4): (1) the Ben Suardal limestone, a dark limestone sometimes containing chert layers and nodules; (2) the Beinn an Dubhaich dolomite, which is only exposed at the highest metamorphic grades (not shown on map); and (3) the Strath Suardal dolomite, a dark gray dolomite containing chert nodules, pipes, and bands. Although calc-silicate minerals and some nodules can be found intermittently throughout the entire aureole, the outcrops studied are in a zone of Strath Suardal dolomite that lies to the south and east of Ben Suardal.

The outcrops start about 0.80 km northeast of the summit of Ben Suardal and run southwest closely following the 600-foot contour below the summit. Although outcrop is not continuous, this zone runs to within eight meters of the granite and contains chert nodules in all stages of metamorphism.

The lithostatic pressure at the time of the granitic intrusion can be estimated from the thickness of the stratigraphic section above the Durness limestone. Nowhere on Skye is the complete section exposed. However, it can be found in two locations less than 15 km apart (see Hoersch, 1978, for details). The thickness from the top of the Durness limestone to the top of the Cretaceous section, which represents the maximum sedimentary overburden possible at the time of granitic emplacement, is 937 m.

If an average rock density of 3.0 g/cm^3 is assumed, then the 937 m section represents 276 bars of lithostatic pressure. Further evidence for the pressure and hence thickness of overburden comes from Brown (1963), who compared an experimental hydrous melting curve for a Skye granite, which crops out approximately 5 km northwest of the Beinn an Dubhaich granite and is only slightly older, with the hydrous quartz–tridymite inversion curve of Tuttle and England (1955). The chill zone of the granite Brown studied contains 2% tridymite, so that the intersection of the two curves gives an estimate of the maximum water pressure (275 kg/cm^3) at the time of intrusion, giving a depth of overburden of 1 km, assuming a density of 3.0 g/cm^3 for the cover. This figure agrees well with the depth and pressure calculated for the Beinn an Dubhaich granite from the stratigraphic column.

At the time of intrusion, basalt could also have overlain the area southeast of the Cuillin Hills, including the area above the Beinn an Dubhaich granite. The maximum depth of basalt over northern Skye is approximately 1220 m (Anderson and Dunham, 1966). If 1220 m of basalt are added to the 937 m stratigraphic section in southern Skye, and still assuming an average rock density of 3.0 g/cm^3, lithostatic pressure could have been as high as 635 bars. Brown's data do not preclude a pressure of this magnitude, since other Skye granites contain quartz instead of tridymite.

Methods of study

Microprobe analyses were done on the automated MAC electron microprobe at the Geophysical Laboratory of the Carnegie Institute of Washington. Standards used for silicate analyses at the Geophysical Laboratory included synthetic manganese glass, nickel olivine, diopsides, orthoclase, and chromium glass, and natural olivine and apatite. Standards used for carbonate analyses were obtained from Dr. Phillip Orville of Yale University and were Iceland spar, ankerite, and dolomite. Data were reduced using a Bence–Albee correction scheme. Analytical errors are approximately ± 2 percent.

To check for compositional zoning in individual minerals, traverses of four to ten spots were made across a few grains in each thin section. No zoning was detected in any mineral so one to six (usually two or three) spot analyses were run at adjacent regions on each grain.

Table 1 lists symbols and abbreviations used in this paper.

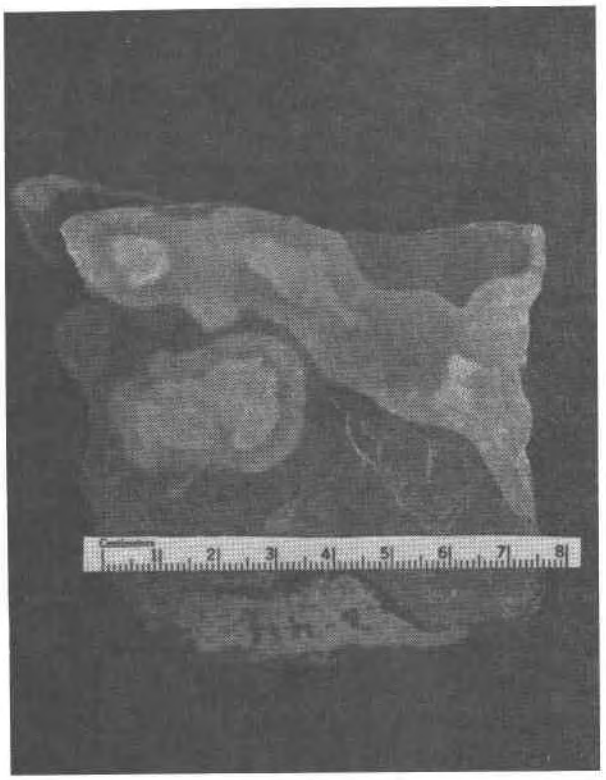

Fig. 2. Metamorphosed chert nodule in dolostone showing growth of radial concentric layers of tremolite, calcite, diopside, and minor dolomite around one nodule and several others in close proximity, 1275 m from intrusive contract. Cores of nodules are composed primarily of calcite and tremolite.

Morphology of nodules

Unmetamorphosed chert nodules vary greatly in shape, ranging from nearly spherical forms to highly irregular, interconnected, pipe-like structures. They range from minute patches less than one mm in di-

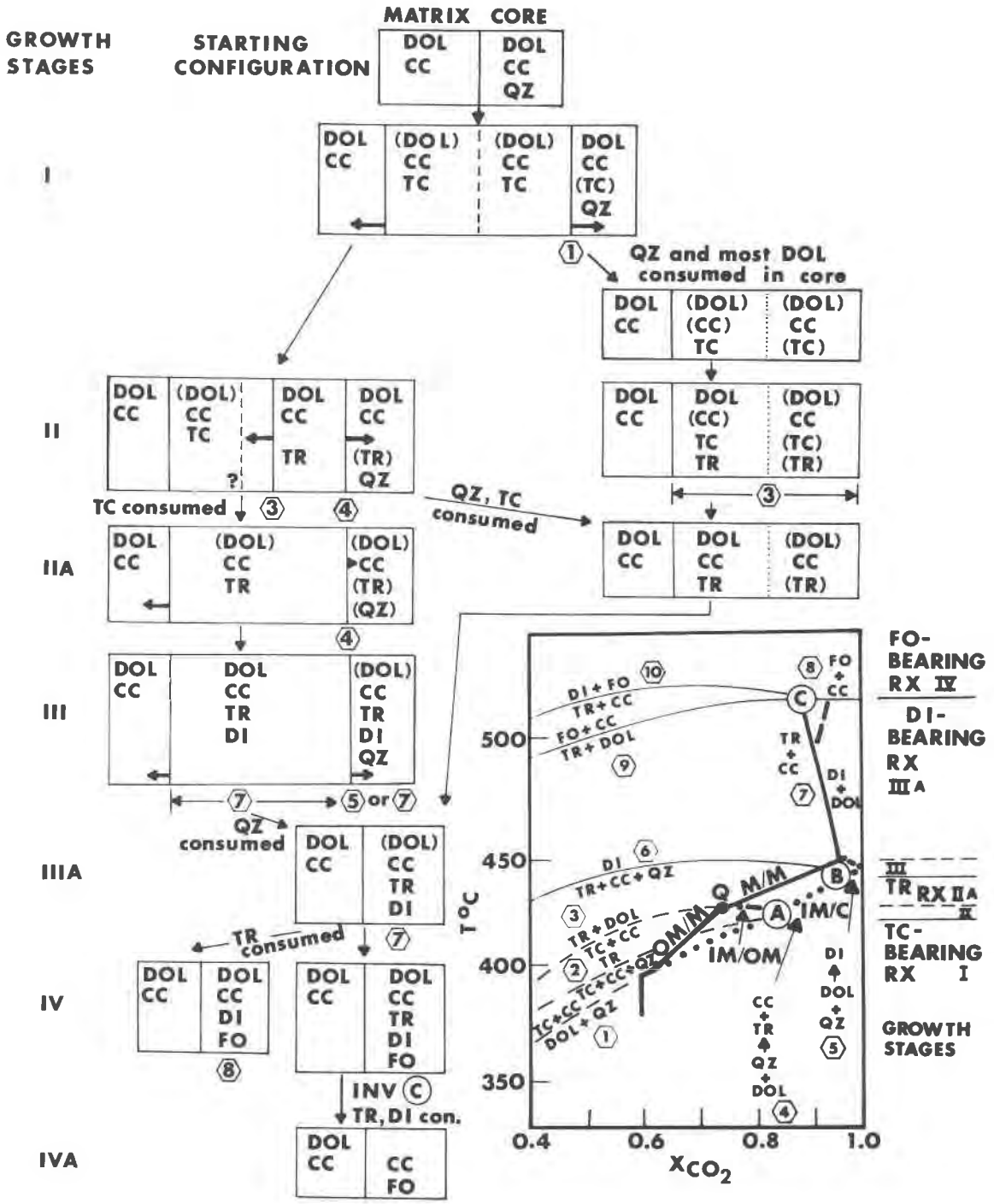

Fig. 3. Stages in the growth of reaction rims around the chert nodules. Arrows within nodules indicate the direction of growth of the reaction rims at each stage. The light dashed line delineates the original nodule boundary. The light dotted lines indicate a discontinuity in the modal amounts of talc and calcite. Parentheses indicate that minor amounts of phases are present. Widths of the reaction rims are not to scale. See Fig. 11 for reactions on T-$X(CO_2)$ diagram. Symbols used on the T-$X(CO_2)$ diagram are: IM/C=inner mantle–core boundary, OM/M=outer mantle–matrix boundary, IM/OM=inner mantle–outer mantle boundary, M/M=mantle– matrix boundary.

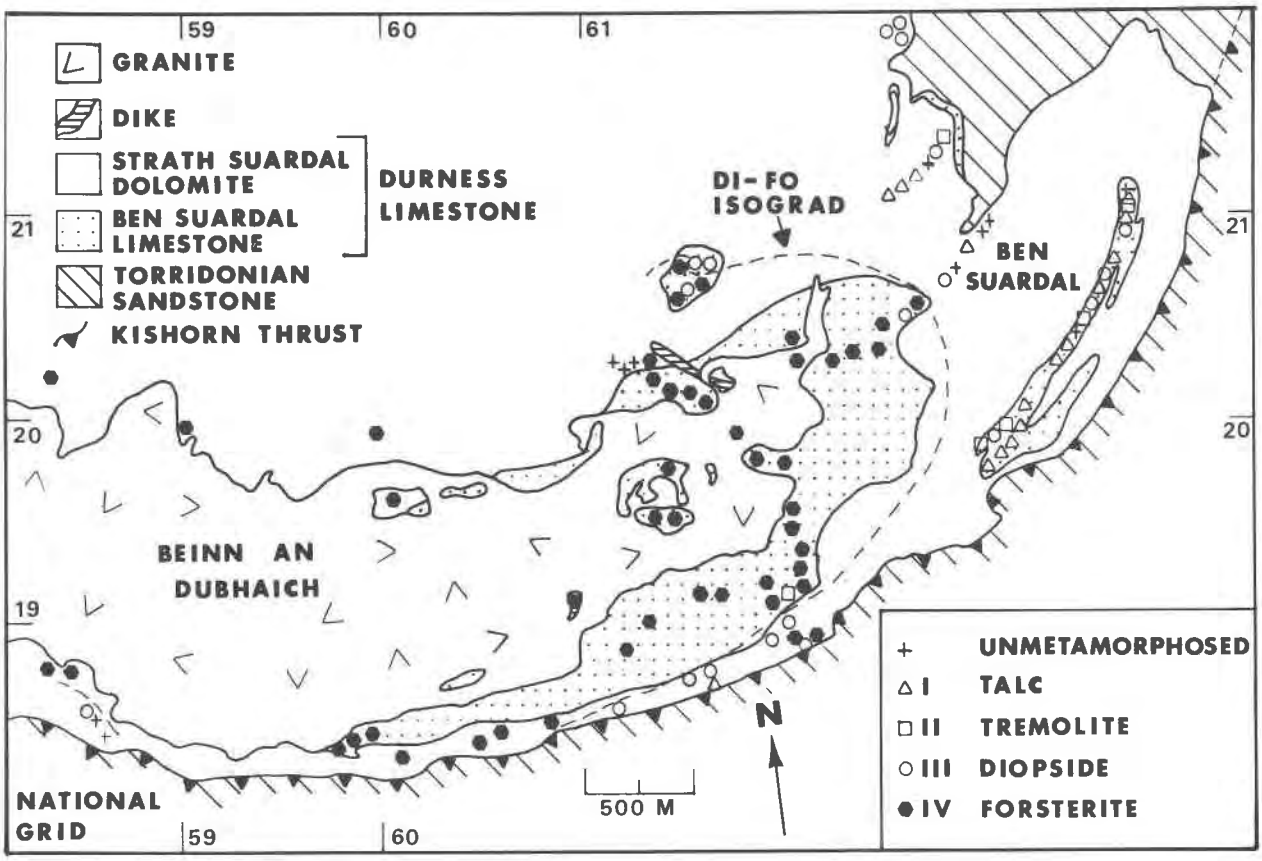

Fig. 4. Geologic map of the Beinn an Dubhaich area showing distribution of metamorphic stages and horizons of the Durness limestone.

ameter to pipes 10 to 30 cm long and 2 to 4 cm wide. The concentration of nodules in the dolostone ranges from <1% to >30%.

During metamorphism irregularities on the outside of the nodules are smoothed by the formation of calc-silicate minerals producing either fairly straight or curved boundaries, depending on the original shape of the nodule (Fig. 2). If two nodules are in close proximity, the new mineral layers may grow around both of them, further enhancing the smoothing process. Generally these new mineral layers grow parallel to the original boundaries between the chert and the matrix so that in spherical or elliptical nodules the calc-silicates grow in concentric radial layers.

Petrography of unmetamorphosed nodules of the Strath Suardal dolomite

Unmetamorphosed chert nodules in the Strath Suardal dolomite are composed of 65–80 percent microcrystalline to cryptocrystalline quartz. The other 20–35 percent consists of calcite and dolomite aggregates, veins, fossil remnants, and dolomite rhombohedra.

The matrix surrounding the unmetamorphosed nodules is monotonously regular dolostone containing 99 percent dolomite, 1 percent calcite, and trace amounts of carbonaceous material and opaques. The contacts between the dolostone matrix and chert nodules are sharp, and are marked by either an extremely thin layer of carbonaceous material, a thin layer of calcite, or turbid layers containing large numbers of fluid inclusions.

Stages of metamorphism

Table 2 lists typical assemblages present in the reaction rims of nodules in the Strath Suardal dolomite zone on the southeast side of Ben Suardal (Fig. 1).

The sequence of evolution of the nodule rims can conveniently be divided into four stages, based on

Table 1. Abbreviations and symbols

Phases			
Cc	= calcite	M	= magnesite
Di	= diopside	Qz	= quartz
Dol	= dolomite	Tc	= talc
Fl	= fluid	Tr	= tremolite
Fo	= forsterite		

mineral assemblages found in the nodules, defined in the following way:

(I) talc-bearing assemblages (Tc + Dol + Cc and Tc + Dol + Cc + Qz),
(II) tremolite-bearing assemblages (Tc + Tr + Dol + Cc and Tr + Dol + Cc + Qz),
(III) diopside-bearing assemblages (Di + Tr + Dol + Cc and Di + Dol + Cc + Qz),
(IV) forsterite-bearing assemblages (Fo + Tr + Dol + Cc, Fo + Tr + Di + Cc, and Tr + Di + Fo + Dol + Cc).

The first three stages each contain two assemblages which correspond to minerals found in two different parts of the nodule reaction rims. The first assemblage represents coexisting minerals at either the outside edge of the reaction rim or within the rim itself. The second assemblage represents coexisting minerals at the boundary between the reaction rim and the unreacted core of the nodule. The last stage consists of three different mineral assemblages in association with forsterite. The above stages are shown schematically in Figure 3 and will be discussed in following sections.

In the field it should be possible to map four isograds based on the above stages. Figure 4 shows the distribution of these assemblages. It is only possible to draw the forsterite isograd on the map. Lack of outcrop, lack of quartz-bearing rocks, and fluctuation of metamorphic grade (to be discussed later) prevent definition of the other three isograds at the map scale.

Stage I: talc-bearing assemblages

The first metamorphic reaction observed is the growth of talc and calcite at the boundary between the dolostone matrix and the chert. The talc and calcite grow at the expense of quartz within the nodules and dolomite of the matrix so that a zone consisting of talc, calcite, and minor dolomite widens both into the nodule and out into the matrix (Figs. 3 and 5). In

Table 2. Typical mineral assemblages present in nodules of the Strath Suardal dolomite zone below the summit of Ben Suardal. Assemblages in each nodule are listed from left to right in the following order: matrix, layers of the reaction rim, and core. Combining assemblages of adjoining layers gives minerals coexisting at zone boundaries. Matrices of samples at tremolite grade and higher may contain minor calc-silicate minerals. (a) List of unmetamorphosed nodules, talc-, tremolite-, and diopside-bearing assemblages; (b) List of forsterite-bearing assemblages.

Table 2a.

Sample #	Distance from Granite (m)	Matrix Dol Cc	Tc Dol Cc	Tc Tr Dol Cc	Tc Dol Cc Qz	Tr Dol Cc	Tr Dol Cc Qz	Di Tr Dol Cc	Core Qz Dol
Unmetamorphosed Nodules									
169	2330	X							X
Stage (I): Talc-bearing Assemblages									
171	2214	X	X						X
178	2102	X			X				
181	1942	X			X				
186	1875	X	X						X
187	1839	X	X						X
203	1442	X	X		X				
200	1400	X	X						X
201	1400	X	X						X
46	1290	X	X						X
35	1207	X	X						X
36	1207	X			X				X
36(1)	1207	X	X						X
38	1207	X	X						X
223	965	X	X						X
224	888	X	X						X
Stage (II): Tremolite-bearing Assemblages									
173	2179	X		X		X			
182	1920	X		X		X			X
194	1647	X		X		X	X		
78	1646	X		X					X
76	1618	X				X			
246	878	X				X			
Stage (III): Diopside-bearing Assemblages									
188	1779	X		X		X		X	X
189	1725	X	X			X		X	X
190	1682	X	X	X				X	
191	1682	X	X	X				X	
193	1659	X						X	X
49	1298	X						X	X
47	1298	X						X	
44	1276	X						X	
262	1030	X						X	X
254	897	X						X	X
248	885	X						X	X
15	567	X						X	
306	556	X			X			X	X
303	369	X						X	

Table 2b.

Sample Number	Distance from Granite (m)	Matrix Dol Cc	Fo Tr Dol Cc	Fo Tr Di Cc	Tr Di Fo Dol Cc	Fo Di Cc	Core Fo Cc
Stage (IV): Forsterite-bearing Assemblages							
21	613	X			X		
4	567	X			X		
310	201	X	X				
311	184	X		X			
313	168	X					X
312	151	X				X	
314	30	X	X	X		X	X
316	8	X					X

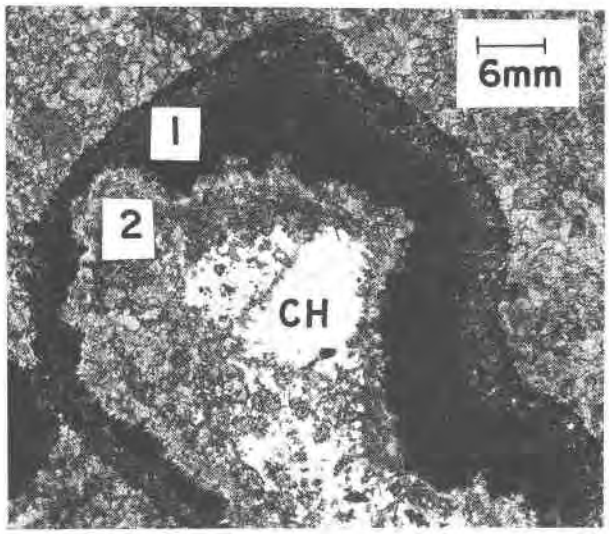

Fig. 5. Photomicrograph of chert nodule within dolostone showing a reaction rim of talc and calcite. The dark part of the reaction rim is growth within the dolomite matrix (1); the light part is growth with the chert (2). The clear part in the core of the nodule is chert (CH). Sample is 88 m from intrusive contact.

a few samples the original insoluble residue boundary is retained in the center of this zone and the new growth can be seen on either side. There is a distinct difference in color between talc grown in the matrix and in the nodule. Talc growing within the nodule is commonly coarser, more platy, and more transparent than that growing in the dolomite; talc growing within the dolomite is finer and appears much darker and more turbid due to fluid inclusions in the dolomite (Fig. 5). I will refer to the zone of the talc growth in the chert as the inner mantle and that in the matrix as the outer mantle. In nodules with a well-defined boundary between the inner and outer mantles, the inner mantle is characteristically richer in talc than the outer mantle (see modes, Table 3). Besides growing at the chert–dolomite boundary, talc can also grow within dolomite rhombohedra, aggregates, and veins in the chert.

At higher grades of metamorphism the rim of insoluble residue may be completely disrupted so that the original boundary between the chert nodule and the dolostone matrix cannot be discerned. Table 3 also lists whole-mantle modes for nodules in which the original boundary could not be discerned. These modes agree well with average modes for samples in which both inner and outer mantles were counted.

After all the quartz has been used up, the nodules are entirely converted to talc and calcite with minor dolomite (less than 5 percent). Commonly the talc forms an almost monomineralic layer (talc content > 90 percent) around a central core of almost monomineralic calcite (calcite content > 90 percent) (Fig. 6). Even in chert nodules entirely converted to calcite and talc, the original nodule boundary can sometimes be discerned either by a line of insoluble residue or a darkening of the outside layer due to fluid inclusions in the dolomite (Fig. 6).

Talc from the reaction rims is close to the end-member composition (Table 4). The only appreciable impurities are FeO (0.42 wt.%) and CaO (0.34 wt.%).

Accessory minerals include sphene, zircon, and iron oxides, and comprise less than 0.01 percent of the rock.

Table 3. Modal compositions of zones in talc-bearing rocks

Volume Percentages

Sample Number	Zone	Dol	Cc	Qz	Tc	Opaques
38	Matrix	99.0	1.0			
	Outer Mantle	7.8	30.0		62.2	
	Inner Mantle	1.0	24.6		74.4	
	Core	11.8	14.6	71.4	2.0	0.2
	Average Mantle	4.4	27.3		68.3	
181	Matrix	99.0	1.0			
	Outer Mantle	19.6	36.8		43.6	
	Inner Mantle	2.0	33.4		64.6	
	Core	22.4	6.8	70.4	0.4	
	Average Mantle	10.8	35.1		54.1	
224	Matrix	98.4	1.6			
	Outer Mantle	8.2	42.2		49.6	
	Inner Mantle	0.0	21.0		79.0	
	Core	22.6	4.8	70.6	2.0	
	Average Mantle	4.1	31.6		64.3	
36(1)	Matrix	98.6	1.2		0.2	
	Mantle	0.4	34.8	0.2	64.6	
	Core	5.4	6.6	85.2	2.8	
46(1)	Matrix	84.5	11.25		4.25	
	Mantle	2.0	14.2	3.2	80.6	
	Core	11.0	13.4	68.0	7.6	
46(3)A	Matrix	99.4	0.6			
	Mantle	1.8	37.0		61.2	
	Core	14.2	17.4		4.8	
187	Matrix	97.6	2.2		0.2	
	Mantle	3.8	29.6	0.2	66.4	
	Core	14.8	11.9	69.1	4.2	
200	Matrix	97.4	1.8		0.8	
	Mantle	1.8	30.8	0.2	67.2	
	Core	3.0	5.4	90.2	1.4	
201	Matrix	99.2	0.2		0.6	
	Mantle	1.6	33.2	1.2	64.0	
	Core	7.2	7.8	82.0	3.0	
209	Matrix	99.0	1.0			
	Outer Mantle	0.6	31.4		68.0	
	Inner Mantle	4.5	36.1	0.3	59.1	
	Core	13.6	19.4	60.0	7.0	
	Average Mantle	2.55	33.75	0.15	63.55	
223	Matrix	90.8	7.8		1.4	
	Mantle	1.2	37.0	0.4	61.4	
	Core	9.0	4.6	86.4		
46(3)B	Matrix	99.0	1.0			
	Mantle	1.4	41.0		57.8	0.2
	Core	2.4	26.8		70.8	

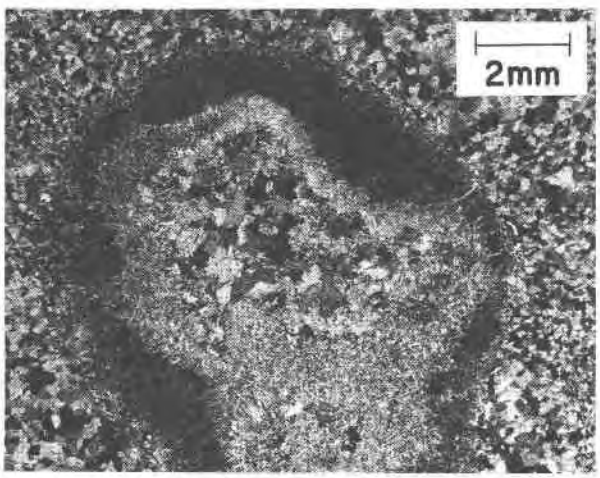

Fig. 6. Photomicrograph of chert nodule completely converted to talc + calcite + minor dolomite. Core is composed primarily of calcite and reaction rim of talc. Boundary where reaction rim darkens probably delineates original chert–dolomite boundary. Sample is 1440 m from intrusive contact.

Stage II: tremolite-bearing assemblages

Tremolite is the second calc-silicate to form, both within nodules in which quartz has been consumed and in those still containing an essentially unmetamorphosed chert core. In nodules containing quartz, tremolite is found within the core of the nodule and along the boundary between the core and mantle. Within the core tremolite is intimately associated with dolomite, calcite, and quartz.

In a few samples a well-defined mantle of tremolite, calcite, and dolomite has formed between the core and another mantle composed of talc, calcite, and minor dolomite. Some of the dolomite appears as blebs within calcite grains and may be the result of exsolution. Other dolomite is found with tremolite needles and laths that impinge the talc–calcite mantle. Stage II of Figure 3 shows the sequence of zones and their corresponding mineral assemblages. At higher grades of metamorphism the mantle of tremolite, calcite, and dolomite widens at the expense of both the core and the talc–calcite mantle. Within the tremolite, calcite, and dolomite mantle, calcite predominates over dolomite near the core. Near the talc–calcite mantle, the amount of dolomite increases.

At more advanced stages of metamorphism, tremolite needles and sheaths can be found throughout the entire talc, calcite, and dolomite mantle, intimately intergrown with dolomite and calcite and embaying talc. A few samples have a mantle consisting entirely of tremolite, calcite, and dolomite, but still retaining a core of unmetamorphosed dolomite, quartz, and calcite (Stage IIA, Fig. 3).

At the most advanced stage of tremolite growth, many nodules are wholly converted to tremolite, calcite, and dolomite, depending on their size. In the same thin section small nodules may be entirely converted whereas larger nodules may still retain a core of quartz, calcite, and dolomite. In nodules in which no core remains, a zonation of mineral proportions commonly persists (Table 5). The mantle contains mostly tremolite with lesser amounts of calcite and dolomite. The tremolite is nematoblastic, forming radial concentric aggregates around the core, which consists primarily of calcite with a few tremolite needles and laths (Fig. 7).

In the outer mantle of samples near the higher-grade limit of the tremolite zone, tremolite becomes larger (up to 2 mm in diameter), stubby, and can be found as either four-sided crystals or as xenoblastic crystals surrounded by dolomite.

Table 4 lists average chemical analyses of tremolite for two samples. Like talc the tremolite is remarkably

Table 4. Average microprobe analyses of minerals in the metamorphosed chert nodules (in wt.%)

Sample Number	talc[b] 46(1)	tremolite[c] 44(1)	tremolite[d] 47	diopside[e] side 4[f]	diopside[g] 21[f]	forsterite[h] 4[f]	forsterite[i] 21[f]
SiO_2	62.2	58.3	58.4	54.6	54.5	42.1	42.7
Al_2O_3	0.08	0.50	0.43	0.49	0.53	0.00	0.01
Fe_TO	0.42	0.45	0.43	0.20	0.18	1.50	1.11
MgO	30.8	24.8	25.0	18.7	18.8	56.2	57.7
CaO	0.34	13.3	13.0	25.7	25.6	0.14	0.04
K_2O	0.01	0.01	0.02	0.00	0.01	0.00	0.01
Na_2O	0.07	0.08	0.07	0.04	0.11	0.00	0.02
MnO	0.00	0.02	0.02	0.00	0.03	0.02	0.03
TiO_2	0.00	0.01	0.02	0.04	0.06	0.05	0.00
NiO	0.01	0.05	0.07	0.03	0.06	0.00	0.02
Cr_2O_3	0.00	0.00	0.00	0.00	0.02	0.00	0.00
Total	93.93	97.52	97.46	99.80	99.88	100.01	101.64
H_2O[a]	4.79	2.21	2.21				
Total	98.72	99.73	99.67				

[a] Calculated stoichiometric H_2O.

[b] Average based on 32 analyses.

[c] Average based on 38 analyses.

[d] Average based on 12 analyses.

[e] Average based on 23 analyses.

[f] Sample contains the five phase assemblages Fo - Tr - Di - Cc - Dol.

[g] Average based on 17 analyses.

[h] Average based on 4 analyses.

[i] Average based on 2 analyses.

Table 5. Modal compositions of zones in tremolite-bearing rocks

Sample Number	Zone	Volume Percentages Dol	Cc	Qz	Tc	Tr	Di	Opaques	Sphene
15	Matrix	87.0	10.4			2.6			
	Mantle	0.8	30.4			68.8			
	Core	2.4	59.8		15.0	21.4	1.4		
44	Matrix	99.0	1.0						
	Mantle	3.2	17.6			64.6	14.6		
	Core	2.2	60.2			24.8	12.8		
47	Matrix	93.6	0.8			4.0	1.6		
	Mantle	8.8	14.8			67.4	9.0		
	Core	3.4	70.4			22.0	4.0		0.2
49	Matrix	99.0	1.0						
	Mantle	0.6	25.0			72.4	2.0		
	Core	13.6	11.2	74.8		0.4			
182	Matrix	99.0	1.0						
	Outer Mantle	1.8	21.2		73.4	3.4		0.2	
	Inner Mantle	3.6	44.2			48.8	3.2		0.2
	Core	5.2	11.8	81.2		1.8			
191	Matrix	99.0	1.0						
	Outer Mantle	1.4	36.4			62.2			
	Inner Mantle	0.8	17.6			79.2	2.2	0.4	
	Core	1.4	37.4			59.8	1.4		
248	Matrix	96.6	1.4	0.4		1.6			
	Mantle	3.2	29.6			67.2			
	Core	9.8	24.1	65.4		0.7			
254	Matrix	86.0	7.0			7.0			
	Mantle	4.6	33.8			57.8	3.8		
	Core	18.4	22.8	58.8					
262	Matrix	99.0	1.0						
	Mantle	1.6	35.6	0.2		62.6			
	Core	10.2	11.4	77.0		1.4			

pure, with only minor amounts of iron and aluminum.

Stage III: diopside-bearing assemblages

Diopside first appears as skeletal crystals cutting across the tremolite needles and sheaths (Fig. 8). Calcite and subordinate dolomite fill interstices between the diopside grains and tremolite needles. In rare cases in which talc still persists in the mantle, diopside also grows across the talc needles and is associated with calcite and dolomite. In samples in which quartz remains in the core, diopside commonly forms from dolomite and quartz. Many cores contain dolomite, calcite, quartz, tremolite, and diopside, but no samples contain all five in mutual contact. Minerals found in mutual contact are diopside + dolomite + quartz and dolomite + diopside + tremolite + calcite. The zonation of mantle and core is shown on Figure 3 (Stage III).

In approximately one-third of the nodules dolomite and quartz in the core do not react to form diopside. This might be a nucleation/fluid problem. Fluids may act as catalysts in reactions in which water is not needed, such as dolomite + quartz = diopside + CO_2. If water-rich fluid from the matrix cannot enter the core easily because of outgoing carbon dioxide and reduced permeability due to the formation of the mantle, diopside may not nucleate readily.

At higher grades the diopside grains found perpendicular to the tremolite needles continue to form. These clumps enlarge to include more and more grains, whose shapes are generally rounded rhombohedra, in parallel crystallographic orientation. Eventually these clumps coalesce into elongate crystals showing typical pyroxene cleavage (Fig. 9). Intimately intergrown with the diopside are large crystals of dolomite. The diopside crystals are often concentrated in the interior of the nodules, with a layer of either calcite or clear dolomite separating them from the matrix. Fractures in the crystals often contain calcite and dolomite. Samples in which diopside crystal growth has been completed consist of large cuboidal or prismatic crystals found throughout the entire nodule, often impinging on one another.

In a few samples diopside has been retrograded to either talc or tremolite along edges and cracks. Retrogression is, however, extremely uncommon in all the nodules.

Most samples at this grade also contain diopside in the matrix, occurring as either xenoblastic grains or as stubby four-sided crystals.

Table 4 lists average diopside compositions from two samples. As in talc and tremolite analyses, diopside is extremely pure, containing only minor amounts of iron and aluminum.

In a few samples closest to the granite (in the dolostone zone directly southeast of the granite), humite and epidote-group minerals can be found in the matrix; they are more common at forsterite grade. The humite minerals are found as flake-like forms or

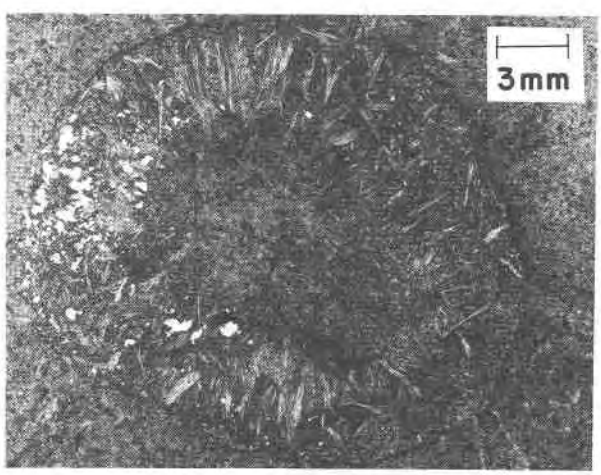

Fig. 7. Photomicrograph showing nodule completely replaced by a rim of radial tremolite needles + calcite and a core composed primarily of calcite. Sample is 1275 m from the intrusive contact.

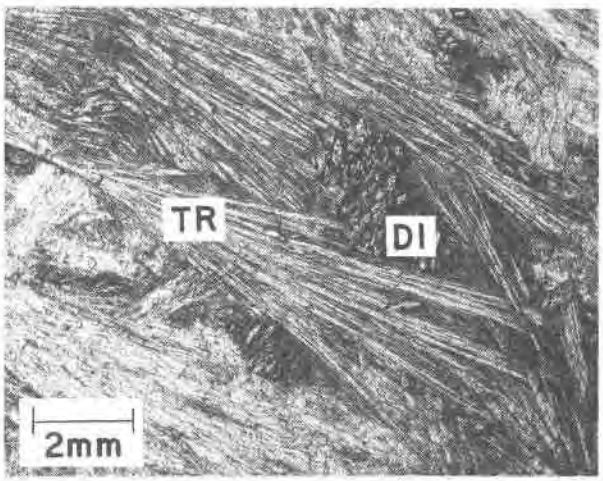

Fig. 8. Photomicrograph showing skeletal diopside crystals growing across tremolite needles and sheaths. Sample is 1225 m from the intrusive contact.

in shreddy aggregates. Epidote-group minerals are found as xenoblastic to rounded crystals.

Stage IV: forsterite-bearing assemblages

Rounded forsterite grains first appear within diopside crystals, along cracks in the diopside, and across grain boundaries between diopside and dolomite (Fig. 10). Forsterite also appears as rounded grains in the dolostone matrix or with tremolite contained within diopside crystals. In all cases calcite is intimately intergrown with or surrounds the forsterite. Figure 3 (Stage IV) shows the assemblages that exist at this grade.

At highest grades of metamorphism, less than 100 m from the granite, nodules contain layers of forsterite in rounded grains plus small amounts of calcite alternating with layers of almost pure calcite. As many as ten layers can be seen in a single nodule. Tilley (1951) thought this layering was due to a Liesegang phenomenon occurring during metamorphism. However, the layering could equally well have formed at the time of initial chert growth; similar alternations of chert and carbonate occur in unmetamorphosed chert nodules throughout the world (Pettijohn, personal communication). This kind of repetitive chert and carbonate layering is found in other places in the Beinn an Dubhaich horizon of the Durness limestone; but here it is never found in its unmetamorphosed state so that its origin cannot be clearly established.

Table 4 lists average chemical analyses of forsterite from the two samples. As in all previously analyzed minerals, the forsterite is extremely pure (Fo = 98.8–99.2) with iron and calcium being the major impurities.

In many samples forsterite has altered to serpentine. At some localities close to the granite (Tilley's marble quarries) ophicalcite has formed where green, waxy veins of serpentine (chrysotile) cross-cut the matrix.

Accessory minerals at this grade include all those seen previously plus brucite/periclase in rounded grains, plagioclase as xenoblastic, twinned patches, and scapolite as elongate laths.

Forsterite-bearing assemblages are the highest-temperature minerals represented in the Beinn an Dubhaich contact aureole other than those of the skarn zone.

Phase equilibria

Based on the mineral assemblages, the contact aureole of the Beinn an Dubhaich granite can be divided into an inner and an outer part. The outer aureole contains the minerals quartz, calcite, dolomite, talc, tremolite, diopside, and forsterite, belonging to the five-component system CaO–MgO–SiO_2–H_2O–CO_2. The inner aureole contains fluorine-bearing minerals (humite-group minerals and idocrase), mainly associated with forsterite and in a few extremely rare cases with diopside. In general this inner aureole contains only the highest-grade forsterite-bearing assemblages, and is less than 100 m from the granite. The presence of the fluorine-bearing minerals suggests that a fluorine-rich fluid emanated from the granite. Fluorine, as measured by microprobe analyses, is not present in the hydrous minerals of the

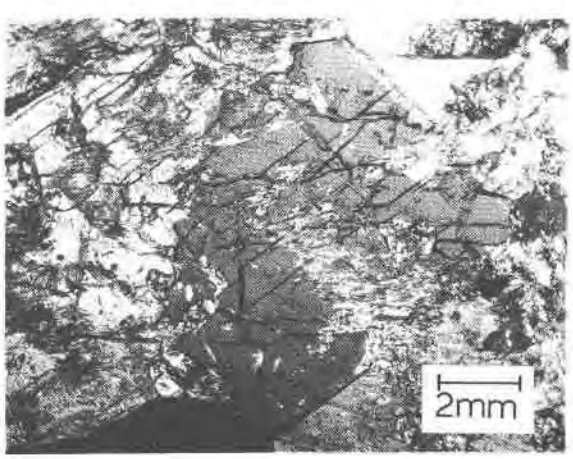

Fig. 9. Photomicrograph of pyroxene crystal in chert nodule surrounding remnants of tremolite sheath. Sample is 567 m from intrusive contact.

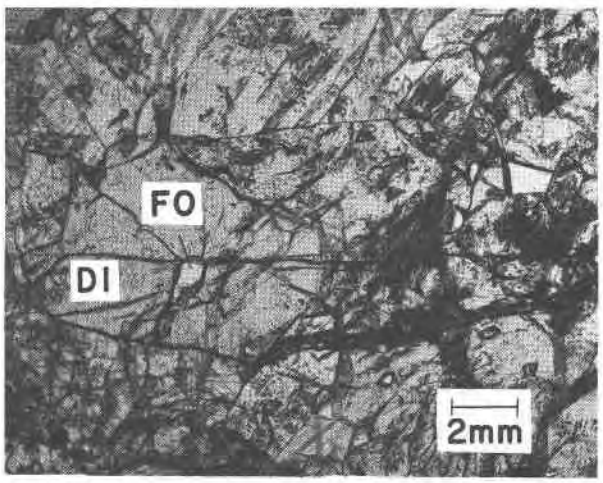

Fig. 10. Photomicrograph showing forsterite grain growing within diopside crystal. Note cracking of diopside crystal due to growth of forsterite. Sample is 567 m from intrusive contact.

outer aureole to any appreciable extent. Table 6 lists average fluorine weight percents for talc and tremolite and the corresponding molecular porportions of each for samples in the Strath Suardal zone below the summit of Ben Suardal. Molecular proportions of fluoro-talc and fluoro-tremolite range from 0.004 to 0.017. Therefore the fugacity of fluorine was low in the outer aureole. CH_4 was also probably not a significant constituent of the fluid phase since only trace amounts of organic material can be found in the samples. As mentioned earlier, the turbidity of the samples is due to a large number of extremely small fluid inclusions and not carbonaceous material. Thus the fugacity of CH_4 was low. Therefore the mineral equilibria may be considered in terms of the five-component system CaO–MgO–SiO_2–H_2O–CO_2. Any fluorine or CH_4 present would of course lower all reaction equilibration temperatures.

Slaughter *et al.* (1975) have compiled the experimental equilibria for the above system. Skippen (1974) has recalculated his thesis (T–$X(CO_2)$ diagrams and included a few more diagrams at lower pressures. Refer to these papers for more detailed discussion and a listing of the equilibria and the data sources.

The ten reactions considered here are shown on Figure 11, the T–$X(CO_2)$ phase diagram at 500 bars total pressure showing relations drawn from Skippen's (1974) paper. There is good agreement between the experimental work of Skippen and Kerrick (personal communication, 1975) for all equilibria but those involving the stability of talc (reactions 1, 2 and 3). Skippen suggests that the talc fields decrease with decreasing pressure and disappear entirely between 500 and 1000 bars total pressure. Kerrick and Slaughter (1976) infer that the talc fields increase with decreasing pressure, taking up more and more space on the T–$X(CO_2)$ diagram. Skippen (1971, 1974) indicates that the limits of error for the pertinent equilibria are quite large, so that the size of the talc fields is subject to considerable uncertainty. Figure 11, showing the stable configuration for the talc fields, was constructed from Skippen's (1974) and Kerrick's (personal communication, 1975) T–$X(CO_2)$ diagrams and by arbitrarily placing invariant point A (Tc–Tr–Dol–Cc–Qz) at $X(CO_2)$ = 0.85; the placement of this point is quite uncertain. The dashed lines are the reactions involving talc. The T–$X(CO_2)$ diagram for the metastable configuration (not shown) is similar to the stable one, except that (1) reaction 4 becomes stable over the entire $X(CO_2)$ range to the left of invariant point B, (2) invariant point A disappears, and (3) reactions 1, 2, and 3 become metastable and appear in reverse order on the diagram; that is, reaction 3 appears at lowest temperatures and reactions 2 and 1 appear respectively at higher temperatures.

The following petrographic and field evidence indicates that talc is stable at low pressures.

(a) The sequence in which the minerals appear in the reaction rims is that shown for the stable talc equilibria on the T–$X(CO_2)$ diagram (Fig. 11), rather than the metastable sequence. Talc first formed by reaction 1, dolomite + quartz = talc + calcite. Tremolite then started to form by reaction 2, talc + calcite + quartz = tremolite, at the inner mantle–core boundary. As soon as a narrow zone of dolomite, calcite, and tremolite formed between the core and the

Table 6. Fluorine analyses of talc and tremolite

Sample Number	Average Fluorine Oxide Weight Percent	Molecular Proportion of Fluoro-talc or Fluoro-tremolite[b]	Distance from Granite-Limestone Contact (m)
Talc-bearing assemblages			
35	0.08	0.017	1207
38	0.03	0.006	1207
46(1)	0.07	0.015	1291
Tremolite-bearing assemblages			
44(1)	0.02	0.004	1276
47	0.08	0.017	1298
76	0.05	0.011	1618
78(2)	0.05	0.011	1646

[a] Analyses done on microprobe

[b] Based on ideal formulae for talc and tremolite

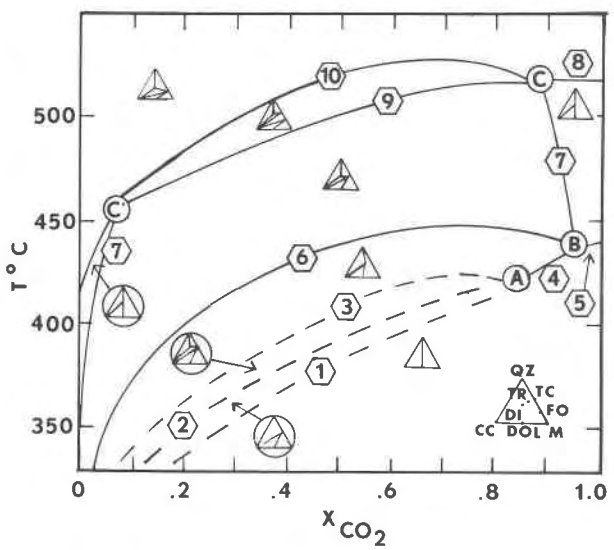

(1) 3 DOL + 4 QZ + H_2O ⟶ TC + 3CC + $3CO_2$
(2) 5TC + 6CC + 2QZ ⟶ 3TR + $6CO_2$ + $2H_2O$
(3) 2TC + 3CC ⟶ TR + DOL + H_2O + CO_2
(4) 5DOL + 8QZ + H_2O ⟶ TR + 3CC + $7CO_2$
(5) DOL + 2QZ ⟶ DI + $2CO_2$
(6) TR + 3CC + 2QZ ⟶ 5DI + $3CO_2$ + H_2O
(7) TR + 3CC ⟶ 4DI + DOL + CO_2 + H_2O
(8) DI + 3DOL ⟶ 2FO + 4CC + $2CO_2$
(9) TR + 11DOL ⟶ 8FO + 13CC + $9CO_2$ + H_2O
(10) 3TR + 5CC ⟶ 11DI + 2FO + $5CO_2$ + $3H_2O$

Fig. 11. T-$X(CO_2)$ diagram at P_T = 500 bars. The solid lines and equilibria taken from Skippen (1974). The dashed lines and invariant point A are stable equilibria arbitrarily drawn on the diagram. See text for details.

mantle of calcite + talc, other reactions took over: reaction 4, dolomite + quartz = tremolite + calcite, at the core–inner mantle boundary, and reaction 3, talc + calcite = tremolite + dolomite, at the outer mantle–inner mantle boundary.

(b) The assemblage tremolite + dolomite + calcite + quartz (reaction 4) is rare, in accord with its limited range of stability in the stable T–$X(CO_2)$ diagram. Likewise, talc-bearing assemblages occur over a wide range of metamorphic conditions, as they should according to the configuration of the stable diagram.

It seems unlikely that talc was stabilized by other components present within the system in view of the small amounts of iron, aluminum, and fluorine present.

The path of progressive metamorphism for the development of reaction rims around chert nodules of the Strath Suardal dolomites can be traced on Figure 11, using the growth stages and reactions shown on Figure 3. The initial composition of the pore fluid is not known, but because talc is stable over such a large areal extent and hence temperature range as well, it was probably fairly H_2O-rich. From the configuration of Figure 11, it must have been somewhere between $X(CO_2)$ = 0.15 and $X(CO_2)$ = 0.85; I will arbitrarily assume an initial value of $X(CO_2)$ = 0.6.

The first stage of metamorphism involved the growth of a mantle of talc + calcite (with minor residual dolomite) by reaction between quartz in the core and dolomite in the matrix (Fig. 3). The mantle grew at the expense of both the core and the matrix. In Figure 3 this growth in two directions is shown by the heavy arrows on zone boundaries; the original matrix–chert nodule boundary is shown by the dashed line. Typical mantles at this stage are less than 2 mm thick, usually 0.5 to 1 mm. This process must have begun when the temperatures reached that of reaction 1 [375°C if $X(CO_2)$ = 0.6, as in Fig. 3 inset]. Initially $X(CO_2)$ values at the inner and outer boundaries of the mantle were probably similar. But as temperature increased and the mantle gradually thickened, $X(CO_2)$ at the core–mantle boundary, where talc, calcite, dolomite, and quartz all coexist, must have followed reaction 1 toward higher values of $X(CO_2)$ (dotted curve in Fig. 3 inset.) $X(CO_2)$ at the mantle–matrix boundary was not constrained to follow reaction 1 because no quartz was present; as the mantle thickened, it probably followed a path like the solid curve in the inset of Figure 3. The path was not at constant $X(CO_2)$ since CO_2 was moving outward towards the matrix–mantle boundary after its release in the rim at the core–mantle boundary. The exact gradient in $X(CO_2)$ across the mantle cannot be specified, but it must have been enough to drive CO_2 outward and H_2O inward for growth of talc at the mantle–core boundary (*cf.* Moore and Kerrick, 1976, p. 517). The reaction at the mantle–matrix boundary was divariant, involving the growth of talc plus calcite at the expense of matrix dolomite plus SiO_2 supplied by outward diffusion from the core.

As metamorphism progressed (stage II), tremolite with calcite and dolomite appeared as an inner mantle between the core and the original mantle of talc + calcite + minor dolomite. This reaction must have begun when the temperature reached that of invariant point A (inset, Fig. 3). As long as quartz (in the core) and talc (in the original mantle) remained in contact, the temperature must have remained at the invariant point. But as soon as a finite layer of tremolite + calcite formed between the talc and

quartz, $X(CO_2)$ at this inner mantle–core boundary was constrained by dolomite, quartz, calcite, and tremolite, and must have followed reaction 4 (stage II, IM/C in inset, Fig. 3), while $X(CO_2)$ at the outer mantle–matrix boundary must have been at some point within the divariant region below curve 3 (OM/M in inset, Fig. 3); reaction 2 was not encountered because no quartz was present at this boundary. As the talc + calcite layer disappeared by reaction, $X(CO_2)$ values at the inner mantle–outer mantle boundary (IM/OM in inset, Fig. 3) and the outer mantle–matrix boundary must have approached one another, converging just as the final talc disappeared (point Q, Fig. 3 inset). Because there is no sign of tremolite having grown at the outer mantle–matrix boundary while talc was still present, the final disappearance of talc must have occurred at a temperature below that of the maximum in reaction 3.

As temperatures increased tremolite + calcite continued to form at the inner mantle–core boundary (stage IIA) by reaction of dolomite and quartz in the core and at the outer mantle–matrix boundary by reaction of matrix dolomite plus SiO_2 supplied by outward diffusion from the core. This reaction at the outer mantle–matrix boundary must have begun after all talc was consumed in the outer mantle and the temperature rose above curve 3; $X(CO_2)$ at this boundary must have followed some path (M/M in inset, Fig. 3) in the divariant region above curve 3. As long as quartz and dolomite were present, $X(CO_2)$ at the inner mantle–core boundary, constrained by dolomite, calcite, quartz, and tremolite, followed curve 4. Most of the tremolite must have formed at this stage, to judge from the relative temperature increments of stages II and IIA; this is confirmed by the scarcity of dolomite in the tremolite mantle.

As metamorphism progressed (stage III, Fig. 3) diopside formed both in the mantle and within the core; the assemblage in the mantle is diopside + calcite + dolomite + tremolite; assemblages of the core are (1) dolomite + calcite + diopside + tremolite and (2) dolomite + diopside + quartz. Reactions must have begun when the temperature reached that of invariant point B (inset, Fig. 3). Both temperature and $X(CO_2)$ were confined to narrow limits while reactions in these two zones took place. $X(CO_2)$ in the mantle, constrained by dolomite, calcite, tremolite, and diopside, followed curve 7. $X(CO_2)$ in the core varied within extremely short distances, being constrained either by dolomite, calcite, tremolite, and diopside along curve 7 or by dolomite, quartz, and diopside along curve 5. As long as quartz and dolomite remained in contact within the core, the temperature must have been below 440°C. At 440°C, as quartz was consumed, the $X(CO_2)$ path in the core converged with that in the mantle along curve 7. $X(CO_2)$ in the entire nodule, now constrained by dolomite, calcite, tremolite, and diopside, must have followed curve 7 (stage IIIA, inset Fig. 3). Beyond 440°C no quartz remained in the core of the nodules.

Note that the mantle was following the CO_2-rich limb of reaction 7 and not the H_2O-rich limb. Evidence to support this conclusion is the sequence of assemblages and hence reactions that have taken place with increasing metamorphic grade. In the aureole the assemblage indicative of invariant point B is closest to the granite–limestone contact and that of A farthest away. Therefore B is the higher-temperature assemblage. For the mantle to be following the H_2O-rich limbs of the curve would require that invariant assemblage A be at higher grade.

As the temperature increased, diopside and dolomite continued to form throughout the nodules at the expense of tremolite and calcite. In those nodules where tremolite was consumed within the nodule, $X(CO_2)$ was no longer constrained by tremolite, calcite, dolomite, and diopside and entered the divariant region below curve 8, following a path similar to that of the dashed line in the inset of Figure 3. When the temperature reached that of invariant point C, forsterite started to form (stage IV), either at the invariant point at the expense of tremolite if it had not been consumed (right box of stage IV), or along curve 8 at the expense of dolomite and diopside if tremolite had been consumed (left box of stage IV, dashed line of inset, Fig. 3).

Three important points should be made about the paths. First, as long as quartz was present, small but significant fluid composition differences existed between core–mantle assemblages and matrix–mantle assemblages. $X(CO_2)$ differences reflect the buffering capacities of mineral assemblages present at zone boundaries, and perhaps the opposing flow of CO_2-rich fluid derived from the reactions outward and H_2O-rich pore fluid inward (see section on talc-bearing assemblages for more detail). Second, mineralogical observations and the T–$X(CO_2)$ diagram suggest that there is a general prograde path that was followed during metamorphism. However, in detail the path varied from nodule to nodule, depending on the size of the original nodule and on how easily fluids could enter the nodules (permeability of the reaction rims). Third, at grades beyond the disappearance of talc, the fluid was CO_2-rich [$X(CO_2) > 0.85$].

Table 7. Microprobe analyses, metamorphic grade, and apparent temperature of equilibration of calcite

Sample Number	35	38	44(1)	46(1)	47	76	78
$FeCO_3$	0.27	0.07	0.12	0.04	0.29	0.08	0.11
$MgCO_3$	2.47	2.22	2.09	2.47	3.18	2.49	2.24
$CaCO_3$	99.24	99.40	98.42	98.69	98.26	101.28	99.74
$MnCO_3$	Tr	Tr	Tr	0.08	0.03	Tr	Tr
Total	101.98	101.69	100.63	101.28	101.76	103.85	102.09
X_{Fe}	0.0022	0.0005	0.0012	0.0003	0.0024	0.0007	0.0009
X_{Mg}	0.028	0.025	0.015	0.029	0.037	0.029	0.026
X_{Ca}	0.9694	0.9740	0.9837	0.9711	0.9604	0.9706	0.9728
$T^{O}C^{a}$	347	323	309	347	406	350	325
Mineral Assemblage Present	Dol Cc Qz Tc	Dol Cc Qz Tc	Dol Cc Tr Di	Dol Cc Qz Tc	Dol Cc Tr Di	Dol Cc Tc Tr and Dol Cc Qz Tr	Dol Cc Tc Tr and Dol Cc Qz Tr

[a]Temperatures obtained from magnesium calcite solvus geothermometry using the equation of Snipes and Price (1976).

This is to be expected since CO_2 was released in nearly all reactions.

From the T–$X(CO_2)$ diagram and the mineral assemblages present at the granite–limestone contact (Tilley, 1947, 1948a, 1951), temperatures at talc grade appear to have been somewhere between 350 and 425°C, at tremolite grade where the reaction dolomite + quartz = tremolite + calcite took place, 425 to 440°C, at diopside grade 440 to 520°C, and at forsterite grade 520 to 600°C [600°C is the temperature determined by Shoji (1975) for the granite–limestone contact based on phase relations].

Attempts to measure fluid compositions directly from fluid inclusions and to determine temperatures from coexisting calcite and dolomite both failed. Fluid inclusions were too small to work with, and it was extremely difficult to find coexisting dolomite and calcite due to the small amount of calcite present in the matrix (1 percent) and the small grain size. Table 7 presents the data from the few thin sections that were analyzed.

Table 7 presents the averaged analyses, their metamorphic grade, and their apparent temperature of equilibration, calculated from the equation of Snipes and Price (1976) derived by a least-squares fit of experimental and observed data. The calcite ranges in composition from 2.09 to 3.18 mole percent $MgCO_3$. The temperatures for talc grade calcites are reasonable (Figs. 3 and 11), ranging from 323 to 347°C. However, both the temperatures calculated for tremolite (325 to 350°C) and diopside (309 to 406°C) grade calcites are too low compared to Figures 3 and 11. The low temperatures might be due to two factors: (1) calcite and dolomite may have re-equilibrated at lower temperatures and (2) dolomite could have exsolved along calcite grain boundaries and been missed in the analyses.

Several final points concern the presence of epidote-group minerals, the alteration of forsterite to serpentine + magnetite in the inner part of the aureole, and the appearance of skarn minerals (andradite, magnetite, wollastonite, *etc.*) within a few feet of the granite–limestone contact. All these features indicate that a water-rich fluid phase was present in the inner part of the contact aureole.

Presumably this fluid phase was derived from volatiles escaping from the crystallizing granite. Wide-scale fluid convection, however, did not occur, as the Beinn an Dubhaich granite has essentially normal $\delta^{18}O$ values for both quartz and alkali feldspars (Forester and Taylor, 1977); these values suggest a low water-rock ratio with little water moving through the system. The presence of skarn minerals (idocrase, andradite, wollastonite, and epidote and humite-group minerals) further suggests that this water-rich fluid carried Al, Fe, F, and possibly some Si. The serpentine after forsterite in the inner aureole also indicates that a very water-rich fluid was present in the late stages of metamorphism (Johannes, 1969; Kerrick *et al.*, 1973). Typically in this reaction the forsterite component of olivine reacted with calcite to form serpentine + dolomite. If any fayalite component was present, iron was released as magnetite.

Fluctuations in metamorphic grade

The fluctuations in metamorphic grade (Fig. 4) could be the result of changing physical conditions (temperature, pressure, and fluid composition) or changing rock composition. Pressure and mineral composition were probably not factors, as pressure gradients are unlikely on the scale of this aureole and mineral compositions do not vary (Table 4). The T–$X(CO_2)$ diagram and the mineral stages (Fig. 3) suggest that the fluctuations were due to changing temperature rather than changing $X(CO_2)$. For example metamorphic grade in the Strath Suardal zone on the southwest side of Ben Suardal (Fig. 4) fluctuates be-

tween talc-bearing rocks and diopside-bearing rocks in which reactions 5 and 7 (Fig. 11) are taking place. These assemblages cannot coexist at the same temperature.

If the variability of metamorphic grade within the aureole was due to varying temperatures, what caused these temperature fluctuations? One possibility is that an igneous body beneath the limestone controlled metamorphic grade. Hoersch (1979) has determined that granite underlies Ben Suardal, the hill which shows these fluctuations. An attempt was made to correlate metamorphic grade with depth to the granite, inferred from cross-sections calculated from ground magnetic surveys (Hoersch, 1979). A positive correlation could not be made, which indicates either that the cross-sections drawn from magnetic data are not precise enough and do not show all the irregularities in the granite's surface, or that temperature does not correlate with simple proximity of the granite, possibly due to inhomogenity of the heat flow. The underlying granite is, however, probably the cause of the temperature fluctuations, even though a positive correlation cannot be made on current evidence.

Conclusions

Microprobe analyses show that chert-bearing rocks of the Durness limestone can be treated by a T-$X(CO_2)$ diagram for equilibria in the system CaO–MgO–SiO_2–CO_2–H_2O. The only appreciable impurities in the minerals are Fe_TO, Al_2O_3, and Na_2O, which are always less than 0.6 weight percent. Fluorine, too, need not be considered, as molecular proportions of fluoro-talc and fluoro-tremolite are less than 0.017.

The sequence in which talc and tremolite assemblages appear in the reaction rims of the chert nodules and their areal extent in the Beinn an Dubhaich aureole indicate that talc was stable at approximately 500 bars, the estimated lithostatic pressure at the time of granitic intrusion. This suggests that the talc stability field on T-$X(CO_2)$ diagrams increases with decreasing pressure, as suggested by Slaughter *et al.* (1975).

Mineralogical observations and the T-$X(CO_2)$ diagram suggest that a general prograde fluid composition path was followed during metamorphism. However, in detail the path varied from nodule to nodule, depending on its size, how long it was heated at each temperature, and how easily fluids could enter. As long as quartz was present, small but significant fluid composition differences [$\simeq 0.1$ $X(CO_2)$] existed between core–mantle and matrix–mantle assemblages. These $X(CO_2)$ differences reflect the buffering capacities of mineral assemblages at zone boundaries, and perhaps the opposing flow of CO_2-rich fluid derived from the reactions outward, and H_2O-rich matrix pore fluid inward. The prograde paths further show that the reactions must have equilibrated at $X(CO_2) > 0.85$ once talc was consumed.

Only one isograd in the metamorphic aureole can be defined, that for forsterite-bearing assemblages. Lack of outcrop, lack of quartz-bearing rocks, and fluctuation of metamorphic grade prevent definition of the other isograds at map scale. The T-$X(CO_2)$ diagram indicates that the fluctuations in metamorphic grade were due to varying temperature, probably caused by an igneous body(ies) underlying the limestone.

Acknowledgments

This paper is part of my Ph.D. thesis at The Johns Hopkins University, Baltimore, Maryland. Financial support was partially provided by NSF grant DES 71-00406-A02 (Earth Sciences Section) (George W. Fisher), a Geological Society of America Research Grant, and two Sigma Xi Grants-in-aid-of research. I thank George W. Fisher for guiding this research and Maria-Luisa Crawford and Douglas Rumble for critically reading the manuscript.

References

Anderson, F. W. and Dunham, K. C. (1966) The Geology of Northern Skye. Memoir Geological Survey of the United Kingdom.

Brown, G. M. (1963) Melting relations of Tertiary granitic rocks in Skye and Rhum. Mineralogical Magazine, 33, 533–562.

Forester, R. W. and Taylor, H. P., Jr. (1977)$^{18}O/^{16}O$, D/H, $^{17}C/^{12}C$ studies of the Tertiary complex of Skye, Scotland. American Journal of Science, 277, 136–177.

Hoersch, A. L. (1978) Zoned Calc-Silicate Nodules from the Contact Aureole of the Beinn and Dubhaich Granite, Isle of Skye, Scotland: A reexamination. Ph.D. Thesis, The Johns Hopkins University, Baltimore.

Hoersch, A. L. (1979) General structure of the Skye Tertiary igneous complex and detailed structure of the Beinn an Dubhaich granite from magnetic evidence. Scottish Journal of Geology, 15, 231–245.

Johannes, W. (1969) An experimental investigation of the system MgO–SiO_2–H_2O–CO_2. American Journal of Science, 267, 1083–1104.

Kerrick, D. M., Crawford, K. E., and Randazzo, A. F. (1973) Metamorphism of calcareous rocks in three roof pendants in the Sierra Nevada, California. Journal of Petrology, 14, 303–325.

Kerrick, D. M. and Slaughter, J. (1976) Comparison of methods for calculating and extrapolating equilibria in P–T–X(CO_2) space. American Journal of Science, 276, 883–916.

Moorbath, S. and Bell, J. D. (1965) Strontium isotope abundance studies and rubidium-strontium age determinations on Tertiary rocks from the Isle of Skye, North-west Scotland. Journal of Petrology, 6, 37–66.

Moore, J. N. and Kerrick, D. M. (1976) Equilibria in siliceous dolomites of the Alta aureole, Utah. American Journal of Science, 276, 502–524.

Puhan, D. and Hoffer, E. (1973) Phase relations of talc and tremolite in metamorphic calcite-dolomite sediments in southern portion of the Damara Belt (South West Africa). Contributions to Mineralogy and Petrology, 40, 207–214.

Shoji, T. (1975) Role of temperature and CO_2 pressure in the formation of skarn and its bearing on mineralization. Economic Geology, 70, 739–749.

Skippen, G. (1971) Experimental data for reactions in siliceous marble. Journal of Geology, 79, 457–481.

Skippen, G. (1974) An experimental model for low pressure metamorphism of siliceous dolomite marble. American Journal of Science, 274, 487–509.

Slaughter, J. D., Kerrick, D. M., and Wall, U. J. (1975) Experimental and thermodynamic study of equilibria in the system $CaO–MgO–SiO_2–H_2O–CO_2$. American Journal of Science, 275, 143–162.

Snipes, D. S. and Price, V., Jr. (1976) Paleotemperature determinations using regression functions relating D-spacing, composition, and equilibration temperatures of magnesium calcite. (abstr.) Geological Society of America Abstracts with Programs, 8, 272.

Tilley, C. E. (1947) Cuspidine from dolomite contact skarns, Broadford, Skye. Mineralogical Magazine, 28, 90–95.

Tilley, C. E. (1948a) Dolomite contact skarns of the Broadford Area, Skye: A preliminary note. Geological Magazine, 85, 213–216.

Tilley, C. E. (1948b) Earlier stages in the metamorphism of siliceous dolomites. Mineralogical Magazine, 28, 272–276.

Tilley, C. E. (1951) The zoned contact-skarns of the Broadford area, Skye: a study of boron-fluorine metasomatism in dolomites. Mineralogical Magazine, 29, 621–665.

Trommsdorff, V. (1972) Change in T–X during metamorphism of siliceous dolomite rocks of the central Alps. Schweizer Mineralogische und Petrographische Mitteilungen, 52, 567–571.

Tuttle, O. F. and England, J. L. (1955) Preliminary report on the system $SiO_2–H_2O$. Geological Society of America Bulletin, 66, 149–152.

Manuscript received, August 13, 1979;
accepted for publication, November 7, 1980.